EMG-Based Variable Impedance Control for Enhanced Haptic Feedback in Real-Time Material Recognition

Elisa Iovene[1], Riccardo Monaco[1], Junling Fu[1], Francesco Costa[2], Giancarlo Ferrigno[1], Elena De Momi[1]

***Abstract*—Advancements in robotic systems hold significant promise for enhancing spinal interventions. Despite this potential, the integration of robotic platforms in spine surgeries remains limited to only a few procedures. This paper presents a variable impedance control scheme within a shared-control framework to enhance haptic feedback during spinal surgeries. The system allows surgeons to guide the robot while dynamically adjusting stiffness based on contact forces and human intent, using electromyography signals. This adaptive control offers real-time guidance during interactions with different materials, serving as a safety measure to safeguard delicate structures encountered during surgical maneuvers. The system comprises a 7-DoF robotic manipulator with a 6-axis force/torque sensor and an 8-channel EMG sensor. Technical validation and a user study assessed performance compared to constant parameter (CIC) and linear variable (LVIC) impedance control methods. Results showed reduced contact force ($-5.065 \pm 1.45\ N$ vs CIC's $-13.72 \pm 6.52\ N$ and LVIC's $-8.73 \pm 2.41\ N$) and in-contact displacement ($0.0074 \pm 0.0018\ m$ vs CIC's $0.019 \pm 0.0068\ m$ and LVIC's $0.0125 \pm 0.0028\ m$), when interacting with delicate materials, minimizing the risk to critical anatomical structures. Additionally, a user survey confirmed that the proposed system improved haptic perception and control while preventing undesired movements during interactions with various tissues and structures.**

***Index Terms*—Medical Robotics, Human-Robot Interaction and Collaboration, Haptics, Impedance Control, Spinal Surgery**

I. Introduction

OVER the last decades, significant advancements have been made in integrating robotic systems into surgical procedures, leading to a rapidly evolving field known as physical Human-Robot Interaction pHRI in medical operations. pHRI allows surgeons to guide robots directly with physical contact and has the potential to revolutionize healthcare delivery. By assisting in intricate and delicate operations, surgical robots can reduce the risk of human error while enhancing precision and improving overall surgical outcomes. Haptic feedback plays an important role in realizing these advancements, ensuring that the surgeon's haptic interactions are both intuitive and precise, ultimately enhancing the overall medical experience. Furthermore, these systems have the potential to shorten the overall duration of surgeries and alleviate the mental and physical workload of surgeons [1].

In the realm of robotic surgery, admittance/impedance control is a commonly used control scheme in pHRI tasks [2]. The primary objective of impedance control is to regulate the interaction between the robot and its environment by regulating the robot's stiffness, damping, and inertia. By modifying these parameters, the robot can appropriately respond to external forces based on the specific task [3]. Numerous studies have explored adaptive impedance control in pHRI, ranging from fixed impedance models to dynamic, state-dependent, and time-varying control strategies. Fixed impedance control often falls short when adapting to human intentions in real-time, making it essential to adjust the robot's parameters dynamically. These adaptations can be based on collaborative task objectives and human physical behavior, enhancing the haptic connection between human and robot for smoother interactions. The selection of appropriate impedance parameters is critical for ensuring system stability and effective human-robot collaboration, allowing the robot to track human movements accurately while minimizing resistive forces. Various control strategies have been developed to account for human intentions during robot interaction, dynamically adjusting the robot's control parameters based on the operator's inferred intentions. Some approaches link human intention with the robot's velocity. [4] employs variable admittance control to enhance the intuitiveness of the robotic system. The admittance parameters are adjusted in response to inferred human intentions categorized into actions such as "accelerate" or "stop," based on velocity and acceleration direction. Similarly, [5] utilizes variable impedance control, continuously modulating impedance parameters according to the operator's behavior inferred from the end-effector's velocity. By real-time adjustments to damping based on velocity, the system enhances responsiveness, ensuring smooth transitions during both fast and slow movements. A distinct variation of variable admittance control adjusts damping based on the power transmitted from the human operator to the robot [6]. Here, forces exerted at the robot's handles are continuously measured using two 6D force/torque sensors, with real-time feedback adaptively rendering the target impedance model. This approach aims to reduce the physical effort required by the operator, especially during tasks involving large or heavy objects. Other methods infer human intention through force/torque (F/T) sensors attached to the end-effector of the

[1]E. Iovene, R. Monaco, J. Fu, G. Ferrigno, and E. De Momi are with the Department of Electronics, Information and Bioengineering, Politecnico di Milano, 20133 Milan, Italy elisa.iovene@polimi.it, riccardo.monaco@mail.polimi.it, junling.fu@polimi.it, giancarlo.ferrigno@polimi.it, elena.demomi@polimi.it

[2]F. Costa is with the Spine Surgery Unit - NCH4 - Department of Neurosurgery - Fondazione IRCCS Istituto Nazionale Neurologico "C. Besta" Milan, Italy francesco.costa@istituto-besta.it

This article has been accepted for publication in IEEE Transactions on Haptics. This is the author's version which has not been fully edited and content may change prior to final publication. Citation information: DOI 10.1109/TOH.2024.3524023

robotic manipulator, capturing operator-applied forces in real-time. In [7], a variable admittance controller was introduced to balance accuracy and compliance in a cooperative micro-manipulator. The system adjusts robot behavior based on the operator's intentions inferred through forces measured by an F/T sensor, ensuring both precision and compliance during different operational phases. In [8], a multilayer feedforward neural network integrates both the robot's Cartesian velocity and the force exerted by the operator to dynamically adjust virtual damping in the admittance controller, optimizing the robot's real-time response to operator actions. Meanwhile, [9] proposes a strategy for orthopedic procedures, where a dynamic reference point connected to the robot's end-effector by a virtual spring enhances the operator's control ability, facilitating precise interaction during complex tasks. Additionally, [10] introduces a target admittance model for hands-on procedures, enforcing a remote center of motion (RCM) constraint to ensure stable robot movement even under varying operator forces. The human force is measured with an F/T sensor at the end-effector, maintaining system passivity and operator safety throughout procedures. While these approaches effectively utilize force sensor data to estimate human intention, they rely exclusively on F/T sensors attached to the end-effector of the robot limiting their ability to differentiate between human-generated and environmental forces. This lack of distinction is particularly critical in tasks requiring high precision and adaptability, especially in dynamic environments with varying mechanical properties. In robotic surgery, various strategies have been developed to adapt robot behavior based on human sensorimotor information, allowing real-time adjustments according to the surgeon's actions throughout different stages of a procedure. By incorporating EMG signals, it becomes feasible to infer human effort and dynamically adjust control parameters, enabling the system to better understand the operator's physical state and intentions. This approach not only provides precise control by distinguishing between human and environmental forces but also enhances the robot's capacity to adapt to complex, variable environments, which is especially crucial in surgical tasks. In [11], a variable admittance controller leverages the coactivation level of arm muscles, measured via EMG signals, to switch between predefined damping values. This facilitates either precise or effortless cooperation based on estimated arm stiffness derived from muscle activation. In [12], a variable impedance control strategy for bilateral teleoperation systems adjusts the robot's impedance in real-time according to the operator's sEMG signals, employing a classifier to interpret varying impedance states based on EMG features, thus allowing the robot to reflect the operator's changing arm dynamics. In [13], hand stiffness is estimated from EMG signals to optimize the robot's motion trajectory using a B-spline-based approach, translating the operator's muscle stiffness into precision adjustments for trajectory optimization. Despite their implementations, these approaches focus solely on human-generated forces, particularly through EMG-based stiffness estimation, without addressing the role of environmental forces. In complex interactions with varying external materials, such as those encountered in robotic surgery, this omission can hinder optimal performance. None of these methods consider the mechanical properties of the surrounding environment, which are essential for dynamically adjusting the robot's compliance to ensure both stability and adaptability in real-world applications. Furthermore, these studies do not establish a direct relationship between EMG signals and the force exerted by the user. In contrast, our paper introduces a novel approach that simultaneously accounts for both human and environmental forces. By considering the mechanical properties of materials in contact with the manipulator, the system dynamically adjusts the robot's compliance, ensuring stability and adaptability in challenging real-world scenarios, particularly in spinal surgery. Additionally, there remains a gap in the literature addressing the specific challenges of spinal surgical procedures, which require precise and stable interaction with diverse tissue types.

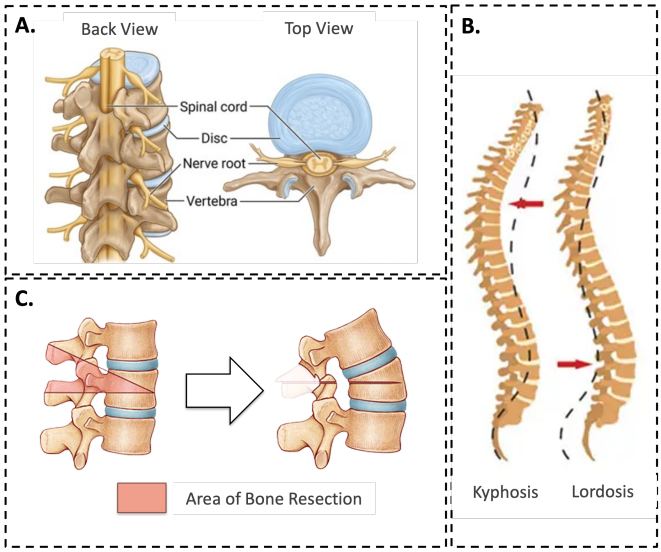

Fig. 1. A. Side (left) and top (right) views of the vertebral structure. B. Example of spinal deformities requiring pedicle subtraction osteotomy (PSO). C. Bone resection area (left) and improved spinal curvature following osteotomy closure (right).

Currently, the application of pHRI in spinal surgery is limited to a small number of specialized procedures, such as pedicle screw placement, where robots have shown effective assistance [14] [15] [16]. However, many complex procedures, including osteotomy, continue to be performed manually using traditional surgical instruments like bone saws, osteotomes, and drills. Vertebral osteotomy, in particular, is a surgical intervention aimed at correcting spinal deformities or improving alignment [17] (Figure 1-B). It typically involves the removal of the posterior elements of the vertebra, along with portions of the vertebral body and pedicles (Figure 1-C). Throughout the cutting and shaping of the bone, surgeons interact with a variety of surrounding tissues, necessitating precise manipulation and careful handling of different materials, including bone, ligaments, and delicate neural structures, to ensure successful outcomes while minimizing the risk of damage to critical anatomical components. In fact, due to the proximity of delicate structures such as the spinal cord and nerves (Figure 1-A), vertebral osteotomy requires a skilled

and experienced surgical team to avoid serious complications, including paralysis [18]. These factors can significantly impact the complexity and duration of the procedure. Additionally, the high level of precision and safety measures required during the surgery can cause significant mental workload and stress for the surgeon. Surgeons also face challenges related to visibility and the dynamic nature of the surgical environment. To mitigate these challenges, intraoperative imaging techniques such as fluoroscopy or intraoperative CT scans are often used to monitor the surgery's status and ensure precision and safety. Nevertheless, these techniques can be time-consuming, expose patients and surgical staff to radiation, and may not offer real-time, high-resolution 3D visualization.

Therefore, the introduction of a robotic system could enhance accuracy, minimize complications, and lower the mental workload for the surgical team. By assisting with critical tasks, robotic systems can help prevent inadvertent damage to surrounding structures, ultimately improving patient outcomes. This work aims to enhance the capabilities of robotic systems for spinal surgical applications, specifically in vertebral osteotomy procedures. We developed a shared control robotic platform that allows users to manipulate the robot with minimal impedance, while it autonomously adjusts rigidity based on contact forces and the operator's EMG signals, modulated by degrees of cocontraction. This collaborative framework allows the surgeon to remain in direct control, which is more suited to open spinal surgeries like vertebral osteotomy, where real-time manual adjustments and precise interactions with exposed anatomical structures are critical. This adaptive approach provides real-time guidance to users during interactions with different materials, acting as a safety measure to protect delicate structures encountered during surgical maneuvers. The human and environmental forces are decoupled by placing the force sensor beyond the point of human interaction with the robot. This enables the sensor to measure external environmental forces while differentiating between the forces exerted by the human and those arising from contact with the environment. Additionally, we ensure system stability through the implementation of a passivity filter, which effectively regulates variations in impedance parameters. The system also generates position feedback upon detecting proximity to critical structures It is worth noting that the proposed variable impedance control algorithm is not specifically optimized for the drilling phase of the osteotomy procedure. As a result, it doesn't directly manage the transition between hard and soft tissues. Instead, its primary function is to assist the surgeon by delivering kinesthetic haptic feedback during contact with various materials, thereby improving the overall interaction experience. The contributions of this study can be summarized as follows:

1) Robotic Assistance in Spinal Surgeries: We explore the integration of robotic platforms to support spinal procedures, considering the mechanical characteristics of the vertebra and its adjacent structures in our control strategy development.
2) Human-in-the-loop: The adaptive strategy incorporates a human-in-the-loop concept by considering both the user's intentions and the real-time force feedback at the end-effector.
3) Usability Evaluation: We conduct a user study to evaluate the effectiveness of our proposed method, comparing it to conventional impedance control strategies.

The paper is structured as follows: the proposed variable impedance control strategy with the stability analysis is reported in Section II. Additionally, in this section, the estimation of the human intention from the EMG signal is presented. Section III illustrates the experimental setup whose results are discussed in Section IV. Finally, limitation and conclusions are reported in Section V and VI, respectively.

II. Methods

A. Impedance Control

The main idea behind impedance control is to modulate the impedance of the system in response to external forces or motions. By adjusting the impedance parameters, namely stiffness, and damping, the desired interaction with the environment can be achieved. For a robotic manipulator with n-joints operating in an m-dimensional task space, the desired impedance control interaction model can be represented as a mass-spring-damper model between the robot and the environment:

$$\mathbf{M}\ddot{\tilde{\mathbf{x}}} + \mathbf{D}\dot{\tilde{\mathbf{x}}} + \mathbf{K}\tilde{\mathbf{x}} = \mathbf{F}_{ext} \tag{1}$$

where $\mathbf{M}$, $\mathbf{D}$, and $\mathbf{K} \in \mathbf{R}^{m\times m}$ are the positive definite inertial, damping, and stiffness matrices, respectively. $\tilde{\mathbf{x}}, \dot{\tilde{\mathbf{x}}}, \ddot{\tilde{\mathbf{x}}}, \in \mathbf{R}^m$, are the position, velocity and acceleration error in Cartesian space, respectively. $\mathbf{F}_{ext} \in \mathbf{R}^m$ represents the total external force exerted on the robot's end-effector, encompassing both the human-applied forces and the interaction forces with the environment.

B. Variable Impedance Control

In this study, a variable impedance control was developed as shown in Figure 2. The proposed adaptive strategy enables real-time adjustment of the stiffness matrix, $\boldsymbol{K}$, in the impedance controller, considering both the user's intention, $\boldsymbol{F}_h$, and the measured force on the end-effector, $\boldsymbol{F}_{ee}$. The damping term, $\boldsymbol{D}$, is indirectly determined by maintaining a constant damping ratio, ξ, such that $\boldsymbol{D}(t) = 2\xi\sqrt{\boldsymbol{M}\boldsymbol{K}(t)}$. Thus, changes in the damping matrix are directly dependent on variations in the stiffness matrix. In our framework, two key assumptions were made: first, the mass matrix $\boldsymbol{M}$ is considered constant [19] [20], and second, both the stiffness matrix $\boldsymbol{K}$ and the damping matrix $\boldsymbol{D}$ are assumed to be diagonal. Moreover, this study focuses on forces acting along the vertical axis (z-axis) of the end-effector, as they have greater significance in osteotomy procedures while keeping the stiffness variation constant for the other two axes. As a result, we employ a simplified notation where the variables are specific to the z-axis (e.g., z_s and F_{ee_z}). This simplification allows equation (1) to be expressed as:

$$m_z\ddot{\tilde{z}} + d_z(t)\dot{\tilde{z}} + k_z(t)\tilde{z} = F_{\text{ext},z} \tag{2}$$

This article has been accepted for publication in IEEE Transactions on Haptics. This is the author's version which has not been fully edited and content may change prior to final publication. Citation information: DOI 10.1109/TOH.2024.3524023

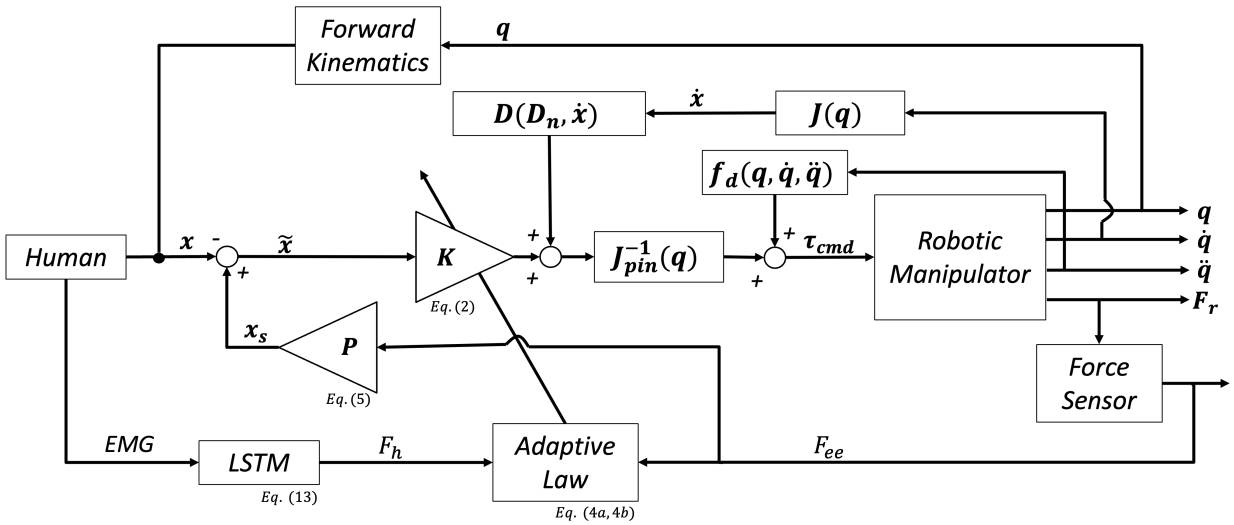

Fig. 2. Scheme of the adaptive impedance control law with safety position feedback: the Cartesian position error, $\tilde{\boldsymbol{x}}$, is calculated by subtracting the current Cartesian pose imposed by the human, $\boldsymbol{x}$ and the safety position feedback $\boldsymbol{x_s}$, generated by multiplying $\boldsymbol{F_{ee}}$ and the gain matrix $\boldsymbol{P}$. This error is multiplied by a variable stiffness matrix $\boldsymbol{K}$, controlled by an adaptive law which receives the human estimated force, $\boldsymbol{F_h}$, derived from an EMG signal and the contact force measured by the force sensor, $\boldsymbol{F_{ee}}$, as inputs. $\boldsymbol{F_{ee}}$ is measured from the force $\boldsymbol{F_r}$ that the robot exerts on the environment. The current Cartesian velocity, $\dot{\boldsymbol{x}}$, is used to compute the damping term $\boldsymbol{D(D_n, \dot{x})}$, where $\boldsymbol{D_n}$ is the normalized damping matrix. The torque command in the joint space $\boldsymbol{\tau_{cmd}}$ is generated by using the Jacobian pseudo-inverse $\boldsymbol{J_{pin}^{-1}}$ and summing the inertial term $\boldsymbol{f}_d(\boldsymbol{q}, \dot{\boldsymbol{q}}, \ddot{\boldsymbol{q}})$. $\boldsymbol{q}, \dot{\boldsymbol{q}}, \ddot{\boldsymbol{q}}$ are the vectors of robot joint position, velocity, and acceleration, respectively.

The stiffness parameter, k_z, is modulated using the following formula:

$$k_z(t) = k_0 + \gamma(t)(k_1 - k_0) \tag{3}$$

where k_1 and k_0 are the limits of range within which the stiffness parameter is allowed to change; the variable gain, $\gamma(t)$, $0 \leq \gamma(t) \leq 1$ $\forall t$, is a function of both the user's estimated force F_h and the measured force on the end-effector, denoted as F_{ee_z}:

$$\gamma = \gamma(F_h, F_{ee_z}) \tag{4}$$

To ensure the desired stiffness behavior in various scenarios, two different γ profiles were developed. The first profile, denoted as γ_1, is specifically designed for interactions with materials that have a high Young's modulus, such as bone. In this case, γ_1 approaches zero, which results in a low stiffness value k_z that is close to the initial stiffness k_0. This low-stiffness setting promotes a compliant behavior, which is crucial for safely interacting with rigid tissues. Conversely, the second profile, denoted as γ_2, is activated when the robot comes into contact with softer materials characterized by a lower Young's modulus. In this scenario, γ_2 approaches one, leading to an increase in the stiffness value k_z. This higher stiffness setting constrains the robot's motion, ensuring precise control during interactions with delicate structures, thereby reducing the risk of damage. The two γ profiles are reported below:

$$\gamma_1(F_h, F_{ee_z}) = \frac{\beta|F_{ee_z}|}{\beta|F_{ee_z}| + ||F_{ee_z}| + F_h|} \tag{5a}$$

$$\gamma_2(F_h, F_{ee_z}) = \frac{\frac{1}{\beta}|F_{ee_z}|}{\frac{1}{\beta}|F_{ee_z}| + ||F_{ee_z}| - F_h|} \tag{5b}$$

with β being a user-chosen tunable parameter. To differentiate between environments characterized by high or low Young's modulus, two conditions were considered: the contact force, F_{ee_z}, and the response of materials to applied forces, Δ_z. When a material with a high Young's modulus is subjected to forces, a high force is recorded, indicating that the material remains undamaged. In contrast, a material with a low Young's modulus starts to deform, resulting in a lower contact force. To capture this distinction, a displacement threshold z_{thresh} and a force threshold F_{thresh} were defined. If the displacement of the robot exceeded z_{thresh} and the contact force was smaller than F_{thresh}, it indicated that the robot was in contact with a material characterized by a low Young's modulus. Consequently, the γ_2 profile was activated in such cases.

Algorithm 1 Conceptual algorithm of the switching strategy

```
No contact
γ(t) = γ1(t)
while |F_ee_z| > 0 (Contact detected) do
    Compute displacement from the contact point
    if |Δz > z_thresh| and |F_ee_z| < F_thresh (Detected contact with delicate structure) then
        γ(t) = γ2(t)
        z_s = ρ F_ee_z
    else
        γ(t) = γ1(t)
        z_s = 0
    end if
end while
```

Moreover, to prevent unintended damage to delicate struc-

This article has been accepted for publication in IEEE Transactions on Haptics. This is the author's version which has not been fully edited and content may change prior to final publication. Citation information: DOI 10.1109/TOH.2024.3524023

tures, the robotic system is needed to counteract the user's movements. This is achieved by generating an additional position command, z_s, which adjusts the end-effector's position based on the external force sensed at the robot's end-effector. Specifically, the feedback position z_s is proportional to the contact force F_{ee_z}:

$$z_s = \rho F_{ee_z} \tag{6}$$

ρ is a constant scalar gain obtained from the gain matrix $\boldsymbol{P}$, shown in Figure 2, as the relation involved only the z-axis. The purpose of this additional feedback is prevent excessive force on soft tissues ensuring the safe completion of the task and it is integrated by modifying the position error term. In the absence of contact, the position error simplifies to $\tilde{z} = z$. However, when contact occurs, the error is adjusted to include the position feedback $\tilde{z} = z_s - z$. This modification ensures that the robot's position is dynamically adjusted based on the interaction forces. A conceptual algorithm of the switching strategy is reported in Algorithm 1.

Finally, to ensure the stability of the system with variable impedance parameters, the methodology proposed in [21] was adopted in this study, where the γ profile was shaped to ensure passivity at every time instant. By adjusting the γ profile according to [21], stability was maintained in the presence of variable impedance control, ensuring a safe and reliable operation of the control system. The proof of stability is reported in the Appendix.

The filter's action is shown in Figure 3 where the robot was moved up and down three times, making contact during each cycle of motion with a soft material (PU).

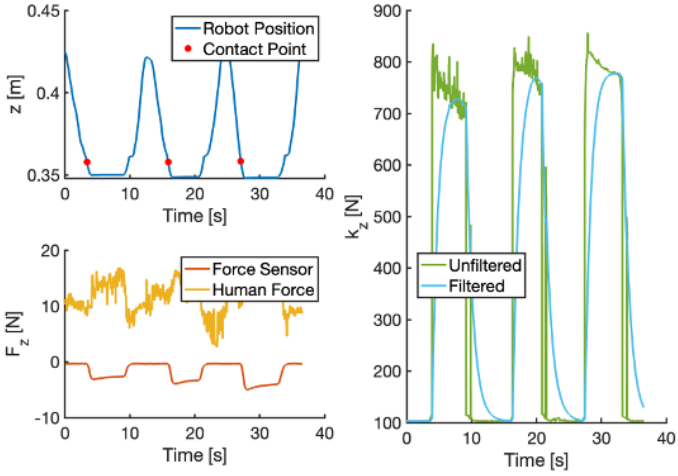

Fig. 3. Top Left: Position of the robot during the experiment, with red-filled circles indicating the contact points. Bottom Left: Forces recorded by the sensor and the human-applied force. Right: Original stiffness values compared to the ones filtered by the passivity filter

Furthermore, the system's stability in the presence of additional position feedback, z_s, was validated using Lyapunov theory [22]. Employing the Lyapunov storage function $V = \frac{1}{2}\tilde{z}^T\tilde{z}$, we ascertain the system's passivity by examining the derivative, $\dot{V}$. If $\dot{V} = \tilde{z}^T\dot{\tilde{z}}$, is negative, the system maintains passivity. The error, $\tilde{z}$, represents the difference between the current position, z, and the safety position feedback, z_s, which is proportional to the force F_{ee_z}. Substituting this error, we obtain:

$$\dot{V} = \tilde{z}^T(\rho\dot{F_{ee_z}} - \dot{z}) \tag{7}$$

To ensure system stability, the feedback gain ρ must be selected such that the rate of change of the feedback force $\dot{F_{ee_z}}$ and the velocity $\dot{z}$ satisfy the stability condition derived from the Lyapunov framework. Specifically, ρ must ensure that the Lyapunov function derivative $\dot{V}$ remains non-positive, thereby guaranteeing energy dissipation and system stability.

To achieve this, ρ is bounded by considering the relationship between the robot's velocity and the rate of change of the contact force:

$$\rho < \frac{\dot{z}}{\dot{F_{ee_z}}},$$

where $\dot{z}$ represents the robot's velocity and $\dot{F_{ee_z}}$ the rate of change of the measured force. This condition ensures that the system dissipates energy and avoids instability caused by excessive force feedback.

C. Human Force Estimation from EMG

In this section, the process of human force estimation is discussed. The goal was to build a model that could accurately map the EMG signals into an interaction force vector $\boldsymbol{F_h}$:

$$\boldsymbol{F_h} = \Phi(\boldsymbol{EMG}) \tag{8}$$

where $\boldsymbol{EMG}$ represents the output signals from 8 EMG channels. Specifically, the model predicts one scalar value that represents the overall force contribution from the muscles, based on the EMG channels as input. The raw EMG signal was first preprocessed: a full-wave rectification was applied to convert the signal into its absolute value. Next, a Butterworth low-pass filter with a cutoff frequency of 5 Hz was utilized to extract the envelope of the original signal. A schematic representation of the EMG signal processing phases is shown in Figure 4. For training the model, a dataset consisting

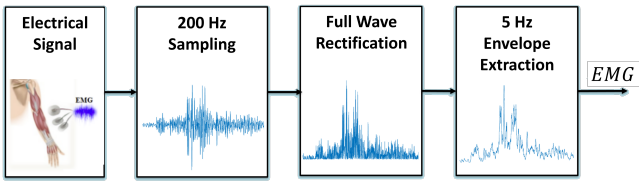

Fig. 4. EMG Signal Processing: Muscle signals are sampled at a rate of 200 Hz. Full-wave rectification is applied, followed by envelope extraction at 5 Hz to obtain the smoothed signal.

of approximately 14,000 data points was collected using 8 EMG sensors placed on the forearm of four different users. This approach was intended to ensure a diverse range of signal data. The users manipulated the end effector of the robot in all directions while keeping the elbow in a fixed position [23]. Throughout the motion, the EMG signals and the force measured by the force sensor on the end-effector were recorded. The dataset was divided into a training set (80 %) and a testing set (20 %). A normalization process

was employed on the training set, scaling the data relative to its maximum values. Participants were instructed to execute maximal voluntary contractions (MVCs) by exerting their peak force on the robot's end effector. The MVCs served as a normalization benchmark for the force signals, ensuring that all recorded data were standardized to a range between 0 and 1. This normalization was similarly applied to the EMG signals. Next, a linear regression was used to weigh the contributions of each EMG channel. Four channels were selected for further use based on their higher relevance in capturing meaningful data. This allowed us to identify the channels that provided the most significant information for our task. In fact, with 8 available EMG channels, not all provide equally useful data [24]. By focusing on the most relevant channels, we were able to reduce the impact of signal instability and cross-talk from less relevant muscles. The processed data was then used to train a neural network, consisting of two Long-Short Term Memory (LSTM) layers, one dropout layer, two dense layers with 64 and 32 units, and one final dense layer with one unit and a sigmoid activation function. Optimal hyperparameters were identified through a comprehensive search for the best hyperparameters. The model was trained for 500 epochs and the Adam optimizer was used. The Mean Squared Error (MSE) and the Root MSE (RMSE) was used to evaluate the performance of the network. The RMSE was normalized by the range of the observed values, enhancing its effectiveness in providing an error measure relative to the variability present in the ground truth data.

III. Experimental Setup

A. Hardware Components

The experimental setup consisted of the following components:

- KUKA Light-Weight Robot 4+ (LWR4+): The robot is equipped with m = 7 Degrees of Freedom (DoFs) and is controlled using the Robotic Operating System (ROS) on Ubuntu 16.04. Communication with the robot is established through the Fast Research Interface (FRI). The synchronization of estimated EMG signals with interaction forces is also managed through ROS, ensuring accurate alignment during data collection. The impedance controller and adaptive law are implemented in C++ and communicated with the FRI at a rate of 200 Hz. The low control frequency remained appropriate for our scenario, defined by slow and deliberate movements, with velocities typically ranging from a few millimeters to tens of millimeters per second.
- Force Sensor: a M3815C six-axis force/torque load cell (Sunrise Instruments) is mounted on the end-effector of the robot. The sensor provided a raw signal with a sampling rate of 1000 Hz which was filtered with an exponential smoothing filter:

$$\boldsymbol{F_{filt_t}} = \alpha_f \boldsymbol{F_{raw_t}} + (1 - \alpha_f)\boldsymbol{F_{filt_{t-1}}} \tag{9}$$

  where $\boldsymbol{F_{filt}}$ and $\boldsymbol{F_{raw}}$ represent the filtered and raw force values, respectively, at time step t. The smoothing factor α_f determines the extent of the filtering and was empirically set to 0.05 providing a balance between effective smoothing and system responsiveness. To obtain only the contribution of the environment on the sensor readings, a compensation of the weight of the tool mounted on the robot's end effector was performed. Due to the non-linear relationship with the end effector orientation, a MultiLayer Perceptron Regressor was trained. A dataset of 14,926 data points was collected by continuously rotating the end effector through various configurations,specifically adjusting its roll and pitch. The dataset was divided into a training set (70%) and a testing set (30%). The training was performed using the orientation of the end effector as input and the filtered force sensor readings, $\boldsymbol{F_{filt}}$, as output. After the training, the network was able to predict the force read by the force sensor, $\boldsymbol{F_{ee}}$, without the tool's gravity contribution at a frequency of 100 Hz.
- EMG Sensor: a Myo Wristband, produced by Thalmic Lab, was used as the EMG sensor. The wristband has 8 channels that capture electric signals produced by the muscles in the forearm. The sensor transmits the raw information over Bluetooth at 200 Hz. The final estimated force F_h is transmitted at 100 Hz.

B. Parameters Tuning

In the control strategy, a stiffness component k_z was varied within a range of $k_0 = 100\ N/m$ to $k_1 = 1000\ N/m$. Since the strategy focuses on the z-axis, the stiffness component of the other axes was kept constant. Specifically, $k_x = k_y = 100\ N/m$, and $k_{rx} = k_{ry} = k_{rz} = 300\ N/m$. To ensure high precision, the damping ratio, d_i, was maintained at 0.8 for all axes (x, y, z, rx, ry, rz). This choice was made to avoid excessive compliance and high-velocity behaviors, which are not necessary in the context of spinal surgery. Furthermore, a weight factor $\beta = 0.1$ was selected to balance the performance requirements of the two profiles, γ_1 and γ_2. This value represents a compromise, aiming for a low γ_1 at high contact forces and a high γ_2 at low contact forces. For the switching logic, we set a force threshold of $F_{thresh} = 15\ N$ and a displacement threshold of $z_{thresh} = 0.005\ m$. These thresholds were chosen after careful empirical consideration across various materials. Choosing a smaller threshold was deemed unrealistic due to real-world factors such as patient movement during procedures, including breathing, and other potential complications that may introduce errors in tooltip position measurements [25]. Conversely, opting for a larger threshold could lead to unsafe procedures by permitting undesired tissue damage before activating the safety strategy. The parameter values are summarized in Table I.

C. Technical Validation

A technical validation was performed to test the accuracy of the neural network in the prediction of the human force and the stability and reliability of the control scheme. The primary objective was to assess the system's ability to maintain stability during contact with various materials. The task involved guiding the robot against a given material and maintaining

TABLE I
CONTROL LOGIC PARAMETER

Parameter	Value
k_0	100 [N/m]
k_1	1000 [N/m]
d_i	0.8
β	0.1
$z_{treshold}$	0.005 [m]
$F_{treshold}$	15 [N]

contact with the material. To evaluate the system's stability, the vertical (z-axis) position of the end effector, z, was recorded to analyze the presence of oscillations and assess the stability of the system. No oscillations were expected as long as contact was kept with the material. To further evaluate the reliability of the control system and test the effectiveness of the control law, 10 repetitions of the same task were performed on different materials. Four materials were carefully selected based on their mechanical properties, specifically their Young's modulus (E), which reflects a material's ability to deform under applied force. The selected materials included: a polyurethane sponge (PU) with Young's modulus of approximately $1-5$ MPa, foam rubber (FR) with Young's modulus of approximately $10-15$ MPa, a polyvinyl acetate (PVA) sponge with Young's modulus of approximately $20-30$ MPa, and a polylactic acid (PLA) vertebra phantom with Young's modulus of approximately $5-10$ GPa. These materials were chosen to mimic the mechanical characteristics of vertebrae, which have a Young's modulus of approximately 15-20 GPa [26], and the surrounding delicate structures with much lower values of around 2-6 MPa [27]. Additionally, a force range from 0 to 25 N was used, based on the maximum force observed during cortical bone cutting at low feed rates (0.05-0.5 mm/s) [28]. Throughout the experiments, the adaptive stiffness, k_z, and the generated position correction, z_s, were also evaluated to test the control system's performance and its ability to adapt to different material characteristics.

D. User Study

The User Study was conducted to evaluate the efficacy of three distinct control modes: Constant Impedance Control (CIC), Linear Variable Impedance Control (LVIC), and the proposed Variable Impedance Control (VIC). CIC provided a baseline with hands-on control with constant impedance. LVIC introduced a dynamic element where stiffness is adjusted linearly within the range of [100-1000] in relation to the displacement of the end-effector after contact with the structure. The objective was to demonstrate that the proposed strategy could prevent users from damaging delicate materials while still enabling effective operation on hard material. Three different materials were used in the experiments: polyurethane sponge (PU), PVA sponge, and the PLA vertebra phantom. Each material was placed inside a box to limit visual feedback on the contact surface. Participants were given specific instructions, which involved guiding the robot through the material, applying force as though they were attempting to perforate it, and maintaining contact for approximately 5 seconds. The assumption was that when encountering a material, they would exert the necessary force to achieve perforation. The task was

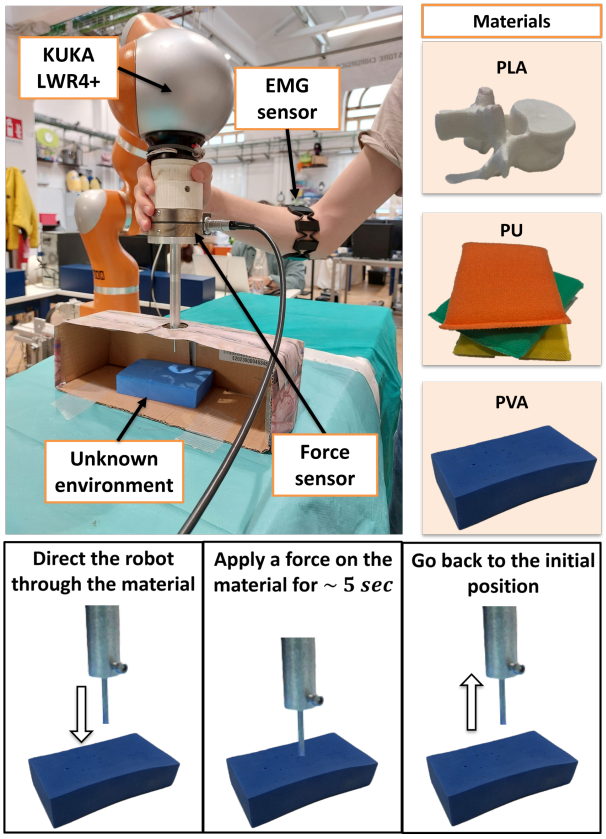

Fig. 5. Top left: the experimental setup for the User Study, where the user guides the robot equipped with a force sensor against various materials placed inside a box. In VIC mode, the user wears the MyoWristband on their forearm. Top right: the materials used during the experiments. Bottom: specific steps of the task.

repeated three times for each material, resulting in a total of nine repetitions per user for all materials. The study included 10 different users, comprising 6 males and 4 females, with an average age of 24.8 ± 2.09 years, all of whom provided informed consent before participating. The experimental protocol was approved by the ethics committee from Politecnico di Milano, Italy (No.2023-5069).

To validate the research hypothesis, two key parameters were analyzed: the contact force, F_{ee_z}, between the robot's end effector and the materials, and the displacement z_d. The displacement was calculated as the difference between the contact point, z_{contact}, and the minimum point reached by the tooltip, z_{min}, as follows:

$$z_d = z_{contact} - z_{min} \tag{10}$$

For each material $m \in [1, 2, 3]$, the average values $\hat{F}_{ee_z}$ and $\hat{z}_d$ were computed according to the following equations:

$$\hat{F}^m_{ee_z} = \frac{\sum_{i=1}^{r} F^i_{ee_z}}{r} \tag{11}$$

$$\hat{z}^m_d = \frac{\sum_{i=1}^{r} |z^i_d|}{r} \tag{12}$$

where $r = 3$ are the repetitions for each user. A lower contact force F_{ee_z} and a lower displacement z_d were expected in

This article has been accepted for publication in IEEE Transactions on Haptics. This is the author's version which has not been fully edited and content may change prior to final publication. Citation information: DOI 10.1109/TOH.2024.3524023

TABLE II
QUESTIONNAIRE

	Statements (S)
S1	The system was easy to use
S2	People can learn to use this system very easily
S3	It is required prior knowledge to use this system
S4	The system was subjected to inconsistency among repetitions
S5	It was easy to damage the materials
S6	I was able to distinguish the different materials
S7	The robot didn't allow me to complete the task with some materials
S8	The task was mentally demanding

case of contact with materials with low Young's modulus when using the proposed strategy. In the case of contact with materials with high Young's modulus, a similar performance between CIC, LVIC, and VIC modes was expected. Moreover, a questionnaire was administered to assess the users' subjective experience during the experiment with the different control modalities. The participants were asked to assign a score from 0 to 5 to each of the statements. The statements of the questionnaire are reported in Table II.

In order to assess the statistical validity of the collected data distributions, the Kruskal-Wallis test, with statistical significance set at 0.05 (p-value < 0.05), followed by a post-hoc Dunn-Sidak test was performed. Figure 5 illustrates the experimental setup employed in the User Study.

IV. Results and Discussion

A. Technical Validation

The following section presents the results of the validation experiment conducted to assess the performance of the system. The human force prediction model has been validated on the remaining 20% of the data. Assessment was conducted using the Mean Squared Error (MSE), yielding a value of 0.015. Additionally, the normalized Root Mean Squared Error (RMSE) was calculated, resulting in a value of 0.0060. The result indicates that the network necessitates enhancement, but it is sufficiently discerning to differentiate between moments of high force application by the user and periods of low or no force. Figure 6 displays the estimated human force. Peaks in the graph correspond to instances where the user exerted force on the robot, causing movement, while lower force readings were recorded when the user's hand was removed and the robot remained stationary.

The stability of the system was evaluated by examining the measured position of the end effector, z_{curr}, upon contact with the material, as described in Section III-C. Figure 7 illustrates the end effector's z-axis position during three consecutive repetitions, along with the corresponding plots of the measured force F_{ee_z}, stiffness k_z, and additional position feedback z_s for comprehensive analysis. The user guides the robot along the z-axis towards the material, establishing contact upon reaching it. During this contact phase, the stiffness, k_z, exhibits an increase, reflecting the system's adaptive response. Moreover, once the displacement exceeds z_{thresh}, the safety feedback is activated, stabilizing the end effector's position around the desired point. As contact is broken, both the stiffness and the feedback position return to their initial values. Despite

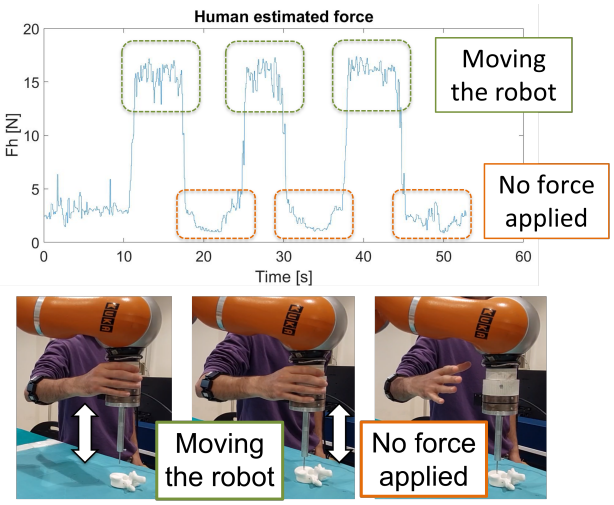

Fig. 6. Human force estimated online using the LSTM-trained model. The predicted force varies between high and low values, reflecting the user's muscle activity.

the transitions between contact and no-contact phases, the system exhibits stable behavior. The adjustments in stiffness and feedback position return to their initial values without any oscillatory behavior. This aligns with the stability analysis conducted, which demonstrates that the control scheme effectively handles contact transitions, ensuring safe interactions with delicate structures. In Figure 8, the boxplot of the adaptive stiffness of the robot and the generated position correction of the 10 repetitions for each material are reported. An increasing stiffness profile, k_z, can be seen in the first three materials, with an average value of $658.28 \pm 221.09\ N/m$ for PU, $624.75 \pm 227.9\ N/m$ for the FR, and $397.5 \pm 195.85\ N/m$ for the PVA. The value recorded in the PVA material is smaller than the one obtained in the other two materials but it is compensated by a higher position correction, which reaches an average value of $0.0339 \pm 0.01\ m$. For PU and for FR,

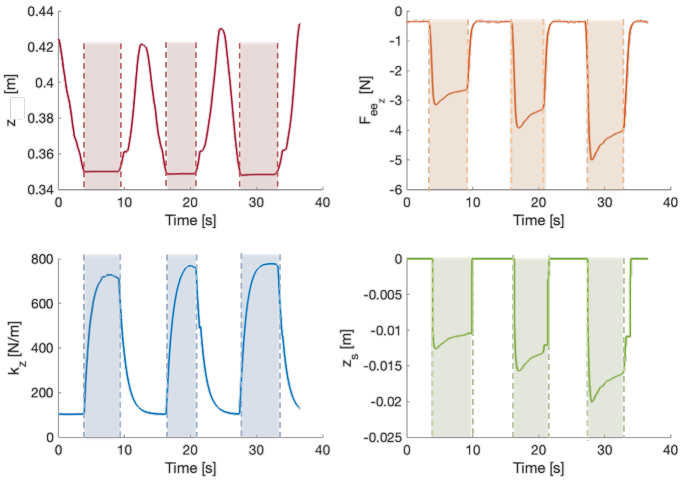

Fig. 7. Response after contact with polyurethane (PU). Upper left: End-effector z position, $\boldsymbol{z}$. Upper right: Contact force, $\boldsymbol{F_{ee_z}}$. Lower left: Robot stiffness, $\boldsymbol{k_z}$. Lower right: Position feedback, $\boldsymbol{z_s}$. Shaded areas indicate the duration of contact.

This article has been accepted for publication in IEEE Transactions on Haptics. This is the author's version which has not been fully edited and content may change prior to final publication. Citation information: DOI 10.1109/TOH.2024.3524023

an average value of the generated position correction, z_s, of $0.0182 \pm 0.0053\, m$ and $0.0267 \pm 0.0083\, m$ was recorded, respectively. It is worth noting the relatively high standard deviations observed in the stiffness measurements, which can be attributed to the low initial stiffness values at the start of each repetition. Considering the PLA vertebra, even though it was not possible to drill it because of the limitations of the setup, the stiffness keeps a low value: $\hat{k}_z = 140.85 \pm 14.88\, N/m$ with a low standard deviation. The test showed that, when contact occurred with materials prone to deformation under low forces, the strategy ensured an increasing stiffness, $\boldsymbol{k_z}$, and the generation of a safety command, $\boldsymbol{z_s}$, both inside the defined ranges.

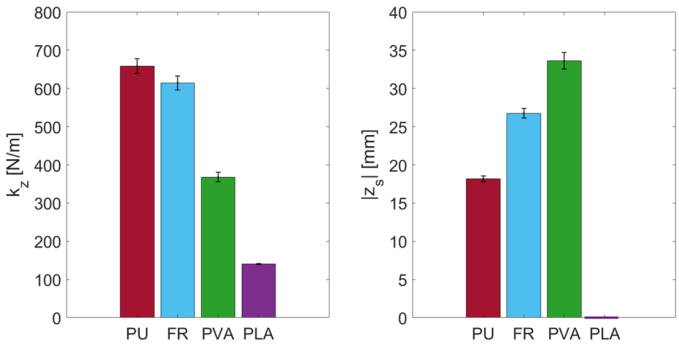

Fig. 8. Boxplots of the variable stiffness k_z (left) and safety position correction $\boldsymbol{z_s}$ (right) across all tested materials.

B. User Study

For each material, the average force and displacement among the 10 users were computed for each modality. In Figure 9 and 10, the boxplots of the displacement and the measured force for each material are shown. The average displacement showed significant differences (p-value < 0.05) between VIC and LVIC modes, and between VIC and CIC modes for Material 1 and Material 2. For Material 1, VIC mode exhibited a mean displacement of $0.0074 \pm 0.0018\, m$, significantly lower than the mean displacement of $0.019 \pm 0.0068\, m$ observed in CIC mode and the $0.0125 \pm 0.0028\, m$ recorded for the LVIC mode. Similarly, for Material 2, VIC mode resulted in a mean displacement of $0.0079 \pm 0.0027\, m$, significantly lower than the mean displacement of $0.0171 \pm 0.003\, m$ in CIC mode. A significant difference was also found when comparing VIC with LVIC mode which resulted in a mean displacement of $0.0134 \pm 0.0033\, m$. These results in terms of displacement show that the proposed strategy is able to recognize the type of material and prevent the user from guiding the robot through it. Significant differences were also observed in the contact force measured on the end effector between VIC and LVIC mode for Material 1, and between VIC and CIC modes for Material 1 and Material 2. For Material 1, VIC maintained a lower average force of $-5.065 \pm 1.45\, N$, compared to CIC's $-13.72 \pm 6.52\, N$ and LVIC's $-8.73 \pm 2.41\, N$. For Material 2, while VIC mode exhibited an average force of $-5.65 \pm 2.57\, N$, significantly lower than the average force of $-14.79 \pm 5.15\, N$ observed in CIC mode, the average force obtained with the LVIC mode, $-7.85 \pm 4.87\, N$, was comparable with the VIC. The reduced force measured in VIC mode demonstrates the system's ability to minimize contact force between the tooltip and the material, effectively reducing the risk of material damage. Results for Material 3 were not statistically significant, with a p-value > 0.05 for both displacement and force in all modalities. This was expected since Material 3 has a high Young's modulus, and the proposed strategy was designed to keep the robot compliant during contact with such materials. Therefore, the results of the study successfully demonstrated that the proposed strategy was effective in preventing damage to delicate materials while still allowing for effective manipulation of materials with a high Young's modulus. Overall, the consistency in reduced force and displacement with VIC across materials suggests that this control strategy is sensitive to the type of material being manipulated and facilitates a user-guided interaction that minimizes the risk of damage, thereby advancing both safety and precision in the task. Our system demonstrated performance that is comparable to several studies in the field of VIC, particularly in its ability to adapt to changing conditions and minimize operational forces. While direct comparisons between these studies and ours are challenging due to the distinct domains, applications, requirements, and tasks, several important parallels and insights can still be drawn. [7] and [8] both implemented variable admittance controllers to optimize precision and force control, similar to our focus. [7] showed reduced operational forces during precise suturing tasks, while [8] achieved higher accuracy with lower effort in a point-to-point task. Despite different applications, these studies highlight the advantages of adapting control strategies in response to task demands, demonstrating how variable control outperforms fixed parameters. Similarly, our VIC approach also focused on balancing precision and force reduction. In both systems, the variable strategy consistently demonstrated better control and force minimization compared to fixed impedance or admittance levels, especially in tasks that demand delicate interaction. [12] proposed a teleoperated framework with real-time adjustable impedance parameters, comparing it with fixed impedance control during contact tasks involving six materials of varying stiffness. They reported that the position deviation decreased as the material became softer, with deviations ranging from 0.41 m to 0.05 m for the stiffest (steel) and softest (sponge) materials, respectively. This trend aligns with our findings, where VIC was particularly effective with softer materials, minimizing contact forces and tool displacement. [12] also recorded lower contact forces with their approach compared to fixed impedance settings, further reinforcing the effectiveness of variable control for precise and safe manipulation. [5] explored a variable impedance control strategy for path-following tasks, comparing it with constant high and low damping settings. They found that higher damping required greater forces to be exerted on the end effector, while low damping facilitated easier movement but resulted in reduced accuracy. Similar to our study, their results highlighted the balance that a variable strategy provides: better accuracy than low damping and reduced force compared to high damping. Our results, in line with these findings, demonstrated VIC's

This article has been accepted for publication in IEEE Transactions on Haptics. This is the author's version which has not been fully edited and content may change prior to final publication. Citation information: DOI 10.1109/TOH.2024.3524023

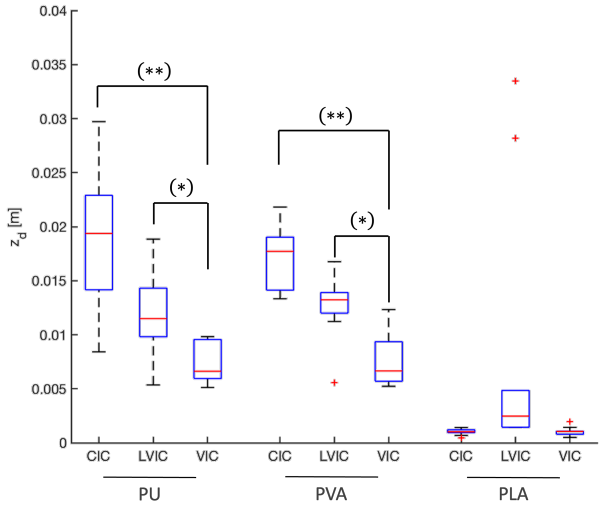

Fig. 9. Comparison of the end effector average displacement among the traditional strategy (CIC), the linear variable strategy (LVIC), and the proposed strategy (VIC), for each material: material 1 (PU), material 2 (PVA), material 3 (PLA). (*, $p < 0.05$, **, $p < 0.01$)

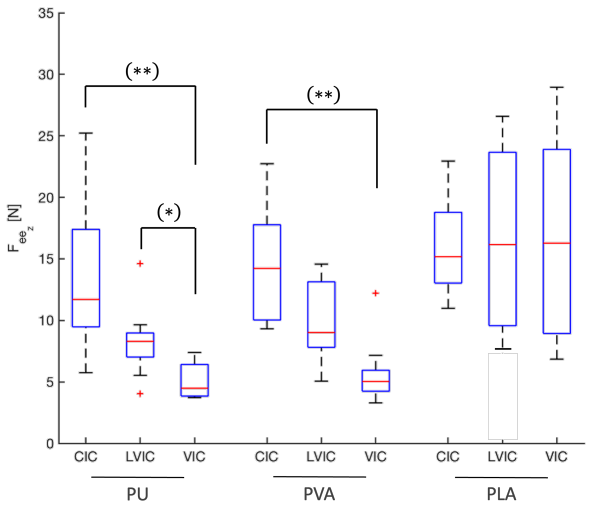

Fig. 10. Comparison of the end effector contact force among the traditional strategy (CIC), the linear variable strategy (LVIC), and the proposed strategy (VIC), for each material: material 1 (PU), material 2 (PVA), material 3 (PLA). (*, $p < 0.05$, **, $p < 0.01$)

ability to minimize contact forces and displacement, especially with delicate materials.

In Figure 11, the results of the questionnaire are presented. The statistical analysis yielded both non-significant and significant results for various statements, shedding light on user perceptions and experiences of the two control strategies under examination. The analysis showed non-significant results (p-value > 0.05) for statements S1, S2, S3, S4, and S8, indicating that the proposed VIC strategy was comparable to the CIC and LVIC in terms of usability, absence of inconsistency, and mental workload. The control strategies demonstrated similarities in key aspects. Participants found VIC, LVIC, and CIC to be equally easy to use (S1), suggesting that the VIC strategy did not introduce additional complexity compared to the traditional approach. Users reported similar ease of learning for both strategies (S2), implying that they were equally intuitive and user-friendly and that no steep learning curve was associated with either strategy. Additionally, there was no significant difference in the need for prior knowledge (S3), and both control strategies exhibited consistency among repetitions (S4). Significant results (p-value < 0.05) were observed for statements S5, S6, and S7, unveiling distinctions in user experiences. Users found it easier to damage materials with CIC and LVIC (S5), indicating that VIC might be considered less likely to cause damage. Users also reported that it was easier to distinguish materials even without visual feedback in VIC mode (S6), suggesting that the strategy effectively simulated a rigid behavior upon contact with a soft material. Finally, users felt the inability to complete the assigned task more often in VIC mode (S7), suggesting that the strategy successfully prevented movement along the z-axis when necessary. This indicates that VIC was more limiting in allowing users to complete the task with certain materials, potentially due to differences in adaptability to various materials or overall performance. In summary, the questionnaire results highlight significant differences in user perceptions and experiences between the control strategies, particularly in terms of material damage prevention, material differentiation, and task completion. These insights provide valuable guidance for choosing the most suitable control strategy and emphasize the importance of user feedback in optimizing the design and performance of robotic systems.

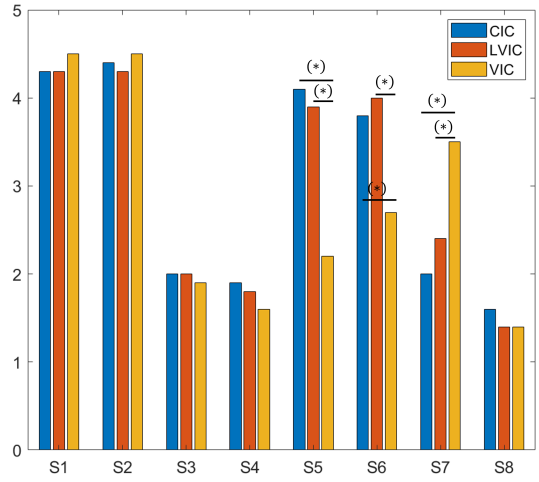

Fig. 11. Barplot displaying the questionnaire results. The x-axis represents the statements (S). The y-axis shows the mean score for each question, averaged across all participants.

V. Limitations

The main limitation of this study is its applicability in a real surgical scenario since the analysis should be performed with a robot equipped with a real surgical instrument. The inclusion of a drill would introduce challenges such as large vibrations which can potentially lead to instability and off-axis forces. Addressing these issues remains crucial for advancing

this early-stage concept into a practical and effective surgical instrument. Additionally, the proposed solution should be extended to include other axes beyond the simple axial one considered. Another significant limitation is the variability in the EMG-based model's performance across users with different muscle strengths. While the LSTM network effectively distinguished between high and low force moments, it struggled to differentiate among varying force levels applied by different users, indicating an area for future improvement. To enhance generalization, we plan to incorporate higher-quality EMG sensors and place electrodes on the shoulder to capture signals from multiple muscles involved in arm motion. Increasing the number of users in our training dataset will also help better account for variations in muscle strength. Furthermore, the use of different soft materials (PU, PVA) in the experiments did not accurately simulate the properties of the spinal cord and blood vessels. Therefore, future experiments should aim for a more realistic experimental setup to enhance the fidelity of the results. Finally, future work should explore the inclusion of ungrounded structures, as this was not addressed in the current study.

VI. Conclusion

In this study, an adaptive impedance controller was developed to allow the recognition of different types of materials. The proposed control strategy strived to replicate the haptic sensations that surgeons traditionally rely on for precise manipulation by changing the stiffness of the robot in real-time. This adjustment was based on the contact force between the robot tooltip and the environment and on the human estimated force, obtained from the EMG signals of the user's arm. Moreover, a safety position command was generated when contact was made with delicate materials. Results showed that the proposed strategy successfully increases the stiffness of the robot when contact is made with delicate materials without causing end effector oscillations, and reduces the risk of damaging such materials, in terms of end effector contact force and displacement, compared to a constant and a variable impedance control strategy. In conclusion, the proposed variable impedance control scheme proved to be a promising approach to improve the safety and precision of spinal surgeries by aligning with the surgeon's haptic perceptions during interactions with various tissues and structures.

Appendix
Proof of Stability

To ensure the stability of the system with variable impedance parameters, a passivity filter was introduced. Specifically, stability is ensured if the following passivity conditions hold:

$$\begin{aligned} 0 &\leq \boldsymbol{K} - \dot{\boldsymbol{D}} \\ 0 &\leq 2\boldsymbol{D}\boldsymbol{M}^{-1}(\boldsymbol{K} - \dot{\boldsymbol{D}}) - \dot{\boldsymbol{K}} + \ddot{\boldsymbol{D}} \end{aligned} \tag{13}$$

Given diagonal matrices, and focusing solely on the z-axis, the conditions of equation 13 can be simplified to:

$$\dot{d}_z - k_z \leq 0$$

$$\dot{k}_z + \frac{2}{m_z} d_z \dot{d}_z - \ddot{d}_z - \frac{2}{m_z} k_z d_z \leq 0$$

To satisfy these constraints, a rate-of-change limit on the variable gain γ is derived, ensuring passivity. This is expressed as:

$$\dot{\gamma} \leq \frac{2(d_0 \delta k + k_0 \delta d)\gamma + 2\delta k \delta d \gamma^2 + 2k_0 d_0}{\delta k + 2d_0 \delta d + 2\delta d^2 \gamma} \triangleq h_1(\gamma)$$

where $\delta k = k_1 - k_0$, as previously defined; $d_0 = 2\xi\sqrt{k_0}$, and $\delta d = 2\xi(\sqrt{k_1} - \sqrt{k_0})$. Moreover, when $\delta d \neq 0$, another passivity condition applies:

$$\dot{\gamma} \leq \frac{\delta k}{\delta d}\gamma + \frac{k_0}{\delta d} \triangleq h_2(\gamma)$$

To ensure that the system remains passive and stable as the desired stiffness γ increases, a passivity filter is introduced to regulate the rate of stiffness change $\dot{\gamma}$. The passivity filter takes as input the desired $\overline{\gamma}_i$ profile and generates an output $\dot{\gamma}_i$ that guarantees system passivity:

$$\dot{\gamma} = \min(h_1(\gamma), h_2(\gamma), \beta(\bar{\gamma} - \gamma))$$

Here, β represents the gain of the filter, ensuring the smoothness of γ_i adjustments.

References

[1] S. W. Wong and P. Crowe, "Cognitive ergonomics and robotic surgery," *Robotic Surg*, vol. 18, no. 110, 2024.

[2] S. Mojtaba, M. Javad K., T. Ali, M. Vivian K., and T. Mahdi, "Impedance variation and learning strategies in human–robot interaction," *IEEE transaction on cybernetics*, pp. 1–14, 2021.

[3] H.-P. Huang and S.-S. Chen, "Compliant motion control of robots by using variable impedance," *The International Journal of Advanced Manufacturing Technology*, vol. 7, pp. 322–332, 1992.

[4] F. Ficuciello, L. Villani, and B. Siciliano, "Variable impedance control of redundant manipulators for intuitive human–robot physical interaction," *IEEE Transactions on Robotics*, vol. 31, no. 4, pp. 850–863, 2015.

[5] A. Lecours, B. Mayer-St-Onge, and C. Gosselin, "Variable admittance control of a four-degree-of-freedom intelligent assist device," in *2012 IEEE international conference on robotics and automation*. IEEE, 2012, pp. 3903–3908.

[6] A. Sidiropoulos, T. Kastritsi, D. Papageorgiou, and Z. Doulgeri, "A variable admittance controller for human-robot manipulation of large inertia objects," in *2021 30th IEEE International Conference on Robot & Human Interactive Communication (RO-MAN)*. IEEE, 2021, pp. 509–514.

[7] H.-Y. Li, T. Nuradha, S. A. Xavier, and U.-X. Tan, "Towards a compliant and accurate cooperative micromanipulator using variable admittance control," in *2018 3rd International Conference on Advanced Robotics and Mechatronics (ICARM)*, 2018, pp. 230–235.

[8] A.-N. Sharkawy, P. N. Koustournpardis, and N. Aspragathos, "Variable admittance control for human-robot collaboration based on online neural network training," in *2018 IEEE/RSJ International Conference on Intelligent Robots and Systems (IROS)*, 2018, pp. 1334–1339.

[9] J. Liang, Y. Yang, Y. Wang, S. Liu, M. Lu, S. Song, and P. Zhang, "Variable admittance control for human-robot collaboration in robot-assisted orthopedic surgery," in *2019 IEEE International Conference on Robotics and Biomimetics (ROBIO)*, 2019, pp. 1544–1550.

[10] T. Kastritsi and Z. Doulgeri, "A controller to impose a rcm for hands-on robotic-assisted minimally invasive surgery," *IEEE Transactions on Medical Robotics and Bionics*, vol. 3, no. 2, pp. 392–401, 2021.

[11] S. Grafakos, F. Dimeas, and N. Aspragathos, "Variable admittance control in phri using emg-based arm muscles co-activation," in *2016 IEEE International Conference on Systems, Man, and Cybernetics (SMC)*, 2016, pp. 001 900–001 905.

[12] J. Li, G. Li, Z. Chen, and J. Li, "A novel emg-based variable impedance control method for a tele-operation system under an unstructured environment," *IEEE Access*, vol. 10, pp. 89 509–89 518, 2022.

[13] L. Biagiotti, R. Meattini, D. Chiaravalli, G. Palli, and C. Melchiorri, "Robot programming by demonstration: Trajectory learning enhanced by semg-based user hand stiffness estimation," *IEEE Transactions on Robotics*, pp. 1–20, 2023.
[14] L. Isador H., L. Isador H., and S. Hesselbacher, "Robotic-assisted pedicle screw placement during spine surgery," *JBJS Essential Surgical Techniques*, pp. 1–15, 2020.
[15] C. Lauretti, F. Cordella, I. Saltarelli, R. Morfino, and L. Zollo, "A semi-autonomous robot control based on bone layer transition detection for a safe pedicle tapping," *International Journal of Computer Assisted Radiology and Surgery*, vol. 18, no. 10, pp. 1745–1755, 2023.
[16] C. Lauretti, F. Cordella, C. Tamantini, C. Gentile, F. S. di Luzio, and L. Zollo, "A surgeon-robot shared control for ergonomic pedicle screw fixation," *IEEE Robotics and Automation Letters*, vol. 5, no. 2, pp. 2554–2561, 2020.
[17] K.-T. e. a. Kim, "Osteotomy of the spine to correct the spinal deformity," *Asian spine journal*, vol. 3, no. 2, pp. 113–23, 2009.
[18] K. C. Kose, O. Bozduman, A. E. Yenigul, and S. Igrek, "Spinal osteotomies: indications, limits and pitfalls," *EFORT Open Reviews*, vol. 2, no. 3, pp. 73 – 82, 2017. [Online]. Available: https://eor.bioscientifica.com/view/journals/eor/2/3/2058-5241.2.160069.xml
[19] K. Kronander and A. Billard, "Stability considerations for variable impedance control," *IEEE Transactions on Robotics*, vol. 32, no. 5, pp. 1298–1305, 2016.
[20] H.-Y. Li, I. Paranawithana, L. Yang, T. S. K. Lim, S. Foong, F. C. Ng, and U.-X. Tan, "Stable and compliant motion of physical human–robot interaction coupled with a moving environment using variable admittance and adaptive control," *IEEE Robotics and Automation Letters*, vol. 3, no. 3, pp. 2493–2500, 2018.
[21] M. Bednarczyk, H. Omran, and B. Bayle, "Passivity filter for variable impedance control," in *2020 IEEE/RSJ International Conference on Intelligent Robots and Systems (IROS)*, 2020, pp. 7159–7164.
[22] H. Mehdi and O. Boubaker, "Stiffness and impedance control using lyapunov theory for robot-aided rehabilitation," *International Journal of Social Robotics*, vol. 4, pp. 107–119, 11 2012.
[23] H. Su, W. Qi, Z. Li, Z. Chen, G. Ferrigno, and E. De Momi, "Deep neural network approach in emg-based force estimation for human–robot interaction," *IEEE Transactions on Artificial Intelligence*, vol. 2, no. 5, pp. 404–412, 2021.
[24] E. Romero Avila, E. Junker, and C. Disselhorst-Klug, "Introduction of a semg sensor system for autonomous use by inexperienced users," *Sensors*, vol. 20, no. 24, p. 7348, 2020.
[25] C. Riviere, J. Gangloff, and M. De Mathelin, "Robotic compensation of biological motion to enhance surgical accuracy," *Proceedings of the IEEE*, vol. 94, no. 9, pp. 1705–1716, 2006.
[26] J. Y. Rho, R. B. Ashman, and C. H. Turner, "Young's modulus of trabecular and cortical bone material: Ultrasonic and microtensile measurements," *Journal of Biomechanics*, vol. 26, no. 2, pp. 111–119, 1993. [Online]. Available: https://www.sciencedirect.com/science/article/pii/002192909390042D
[27] A. P. Ebrahimi, "Mechanical properties of normal and diseased cerebrovascular system," *Journal of vascular and interventional neurology*, vol. 2, no. 2, pp. 155–62, 2009.
[28] K. Matsumiya, Y. Momoi, E. Kobayashi, N. Sugano, K. Yonenobu, H. Inada, T. Tsuji, and I. Sakuma, "Analysis of forces during robotic needle insertion to human vertebra," in *Medical Image Computing and Computer-Assisted Intervention - MICCAI 2003*, R. E. Ellis and T. M. Peters, Eds. Berlin, Heidelberg: Springer Berlin Heidelberg, 2003, pp. 271–278.

Elisa Iovene received her Master's Degree in Biomedical Engineering - Technologies for Electronics from Politecnico di Milano in April 2021. She is currently a PhD candidate at the Department of Electronics, Information, and Bioengineering (DEIB) of the Politecnico di Milano.

Riccardo Monaco received his M.Sc. Degree in Automation Engineering from Politecnico di Milano.

Junling Fu received the B.E. degree in Mechanical Engineering from Guangzhou University and M.S. degree in Mechanical Engineering from South China University of Technology, Guangzhou, China, in 2017 and 2020, respectively. Currently, he is pursuing a Ph.D. degree in the Department of Electronics, Information, and Bioengineering (DEIB) of Politecnico di Milano, Italy. He is a member of the Neuroengineering and Medical Robotics Laboratory (NearLab).

Dr. Francesco Costa served as Associate Professor in Neurosurgery at Humanitas University from February to November 2021. From 2011 to 2021, he worked, first as Assistant Neurosurgeon, then as Section Chief of Spinal Oncology Surgery at Humanitas Clinical and Research Hospital Neurosurgery. He currently holds the position of Head of Spinal Neurosurgery in the Department of Neurosurgery.

Prof. Giancarlo Ferrigno, Ph.D. received the M.Sc. degree in electrical engineering and the Ph.D. degree in bioengineering from the Politecnico di Milano, Milan, Italy. He is a Full Professor of Electronics and Information Bioengineering and the Founder of the Neuroengineering and Medical Robotics Laboratory with the Department of Electronics, Information and Bioengineering, Politecnico di Milano.

Prof. Elena De Momi, Ph.D. received her M.Sc. and Ph.D. degrees in biomedical engineering from the Politecnico di Milano, Milan, Italy. She is currently an Assistant Professor in the Department of Electronics, Information, and Bioengineering, Politecnico di Milano.